EasyChair Preprint

№ 1271

Tactile Inspection of Concrete Deterioration in Sewers with Legged Robots

Hendrik Kolvenbach, Giorgio Valsecchi, Ruben Grandia, Antoni Ruiz, Fabian Jenelten and Marco Hutter

July 6, 2019

Tactile Inspection of Concrete Deterioration in Sewers with Legged Robots

Hendrik Kolvenbach, Giorgio Valsecchi, Ruben Grandia, Antoni Ruiz,
Fabian Jenelten and Marco Hutter

Abstract We present a tactile inspection approach for legged robots which allows for evaluating concrete deterioration in medium to large-sized sewers. The legged robot, to this end, executes a well-defined scratching motion with one limb on the sewer floor. Inertial and Force/Torque sensors implemented in specially designed feet capture the resulting vibration. The data is used with concrete deterioration estimates from professional sewer inspectors to train a support vector machine. We achieved deterioration level estimates within three classes of over 92% accuracy. The dataset, which we recorded during a field test campaign in the sewers of Zurich is made publicly available.

1 Introduction

The swiss sewage system has a total length of over 130 000 km and presents a significant communal investment. Maintaining the sewers is crucial for public health, but also imposes a considerable cost upon the municipalities. Reports from developed countries indicate that most sewage systems have reached half of the average expected lifetime of 80 years. Thus, the focus is shifting towards maintenance and renovation [1]. As a first step towards maintenance, cost-effective and accurate inspection is essential to assess the state of the sewer system.

Sewers have been built successively, with parts of the system being over 100 years old. This process results in a large variety of used materials, sizes, and shapes. Categorization can be made into medium to large sewers, with an inner diameter of more than 800 mm and small sewers, with a diameter down to 100-150 mm. Large sewers are typically made from concrete or masonry and account for around 10%

All authors are with the Robotic Systems Laboratory, ETH Zurich
Leonhardstrasse 21, 8092 Zurich
e-mail: firstname.lastname@mavt.ethz.ch

of the network [2]. Small sewers are typically made from concrete, stoneware or plastics and account for the remaining 90%. Overall, the majority of sewers is made from reinforced and unreinforced concrete, accounting for almost 40% of all sewers [3]. Although the vast majority of small sewers are of a circular or oval shape, most of the larger ones are jaw-shaped, rectangular or of irregular shape.

The rate of deterioration varies and depends on the design and usage of the sewers. Relevant factors are flow rate, slope, wastewater composition, cleaning intervals, and more [4]. An omnipresent disintegration mechanism acting on concrete in sewers is microbial induced corrosion (MIC) [5]. This type of corrosion occurs when sulfate-reducing bacteria found in the biofilm produce Hydrogen sulfide from wastewater, which is absorbed on the moist surfaces of the sewers and creates sulfuric acids. These acids react with the alkaline minerals in the concrete, which leads to the creation of large, expansive minerals and ultimately the loss of structural integrity [6].

The current inspection approaches vary depending on the diameter, material, shape and expected damage to the sewer. For example, small pipes are prone to experience clogging or leaking in contrast to large sewers. Thus, visual inspection is performed by tethered pipe-inspection robots, which crawl through the sewer and sometimes carry tools for removing clogs. Many of such small-scale robots exist and are commercially available [7].

So far, medium to large sewers are inspected by humans with the goal of manually assessing the deterioration level. To assess the deterioration level of the concrete in medium-large sewers, inspectors check the roughness of the concrete visually and tactilely with their hands and feet. As the highest deterioration occurs in the center of the sewer, which is often covered by a biofilm and wastewater, purely visual assessment fails to predict the deterioration reliably. Humans have the advantage to adapt to irregular sewer shapes and can move through pipe diameters down to 800 mm.

However, the inspection tasks at nominal environmental conditions (slippery ground, flowing water, dirty, damp, occasional narrow spaces) are monotonous, dangerous and carry health-risks [3]. Additionally, vast safety precautions such as gas measurements and blocking off large areas of a sewage system before inspection have to be taken, which potentially disrupt the network. Overall, the inspection task presents an excellent opportunity for versatile service robots.

Only a few inspection robots for medium to large diameter sewers have been developed until today. *SVM-RS* from the Fraunhofer Institute for Factory Operation and Automation is a combined cleaning and inspection robot [8]. The robot weighs 3500 kg, has a size of 3500 x 1500 x 1500 mm (L x W x H) and a reach of 1200 m. Various cameras, ultrasonic sensors, structured light line scanners, and temperature sensors are implemented. Redzone robotic's *Responder* is a 300 kg, tracked platform which can be deployed in sewers with a diameter from 915-6000 mm and has a reach of up to 1000 m [9]. The robot is equipped with cameras, laser sensors and ultrasonic sensors for inspection. A robot by the Nanyang Technological University allows for underground excursions in tunnels with a minimum diameter of 3000 mm and lengths up to 400 m [10]. The robot uses cameras and a laser profiler.

The typical method for detecting concrete damages helped by a robot is through an operator who interprets the acquired camera images and ultrasonic or laser sensor data. All robots are tethered and tend to get bigger with increasing operational range due to the required power for pulling the cable. For some of the systems, the deployment through a common utility hole seems questionable. Because of the limited range, traversing through oddly shaped sewers and junctions is not considered. An interesting robot in this context is Pure technology's *SmartBall*, which is a free-swimming robot that can be deployed in a water stream and scans the sewer with ultrasonic sensors to find leaks [11]. However, it has no means of controlling its path and depending on the sewer shape the deployment and capture might be tricky.

We propose the usage of autonomous legged robots to inspect large and medium-sized sewers. Legged robots are relatively small, have high mobility in a complex human-made environment and can adapt their posture to inspect areas of interest [12] [13]. Similar to humans, the robot can probe the environment tactilely by using its limbs, as we have shown in previous work [14] [15].

As part of our contribution, we have successfully deployed the autonomous quadruped robot, *ANYmal* [16], in the sewers of Zurich[1] (Figure 1). With the help of specially designed sensor-equipped feet, we collected a large dataset by performing an inspection motion with one limb of the robot 355 times. The ground truth of the concrete deterioration was provided by sewer inspection professionals to complete the dataset. Later on, we were assessed the level of concrete deterioration with high accuracy using supervised machine learning techniques. Our approach only uses sensors employed in the foot, works reliably on different surface conditions, and outputs the current state, without the need for manual sensor signal interpretation.

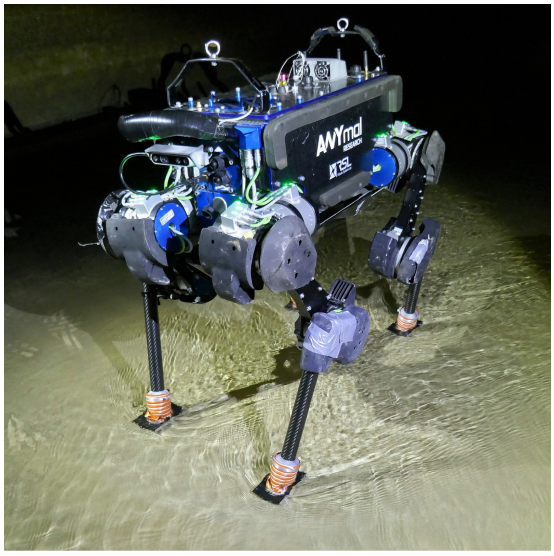

Fig. 1 Depiction of *ANYmal* with custom feet deployed in the sewers of Zurich.

[1] https://youtu.be/fdGKRgVYAtg

This paper is structured as follows. First, we describe the robot with a focus on the foot design in Sec. 2. The tactile inspection motion is explained in Sec. 3. Next, we present the field tests in the sewers and the creation of the dataset in Sec. 4.1. The classification approach and the results are presented in Sec. 4.2 and Sec. 4.3 respectively. Finally, we conclude the work in Sec. 5.

2 Hardware description

ANYmal is a 30 kg quadruped robot driven by twelve series elastic actuators mounted at the joints. The dimensions of the robot are 800 mm x 600 mm x 700 mm when standing and 800 mm x 600 mm x 400 mm with tucked up legs, which allows deployment through a common utility hole. The kinematic structure of the robot is designed to achieve an extensive range of motion, allowing it to overcome obstacles and manipulate the environment. *ANYmal* can operate partially or fully autonomously with on-board batteries. The battery allows the system to traverse up to 3.6 km with a trotting gait at 0.5 m/s on a single charge. Optionally, the robot can be recharged without human interaction by a docking station if long-term autonomy is needed [17].

We designed sensor-equipped, adaptive feet to enhance locomotion on rough and slippery terrains encountered in the sewers while measuring local ground inclination and superficial properties. Similar to the rest of the robot, the feet have to be sufficiently robust to operate continuously in a challenging environment. The design is based on the adaptive foot proposed in previous work of our group [18], which consists of a large flat contact surface that can comply to the local ground inclination without interfering with the kinematics of the leg.

With a possible inclination of the terrain of up to 25°, the range of motion (ROM) for ground compliance is set to 50° around the pitch- and 30° around the roll axis. Since each leg only allows for hip abduction/adduction, hip flexion/extension and knee flexion/extension, the foot compliance around yaw prevent slipping while turning. With a weight of 314 g (including cabling and connectors), it is lighter than both the original point foot and the previous adaptive foot. Figure 2a illustrates the subassemblies of the foot, which are described in the following.

1) Foot sole: The sole has a surface area of 60 cm^2 (100 mm x 60 mm) and is made from an off-road rubber tire featuring 5 mm studs for increased traction (Figure 2b). The sole is connected to a metal rim by clamping, which avoids peeling and gluing issues. A damping foam placed between the rubber sole and the metal structure reduces the peak loads resulting from impact forces during walking. An acetal slider avoids the foot getting stuck on overhanging edges and retains the metal rim.

2) Pivot joint: The pivot joint features a lightweight universal joint with integrated end stops to provide the required ground compliance. It is surrounded by an Ester Polyurethane rubber tube of Shore A70 that provides the retaining force to reset the foot to its initial position after deflection.

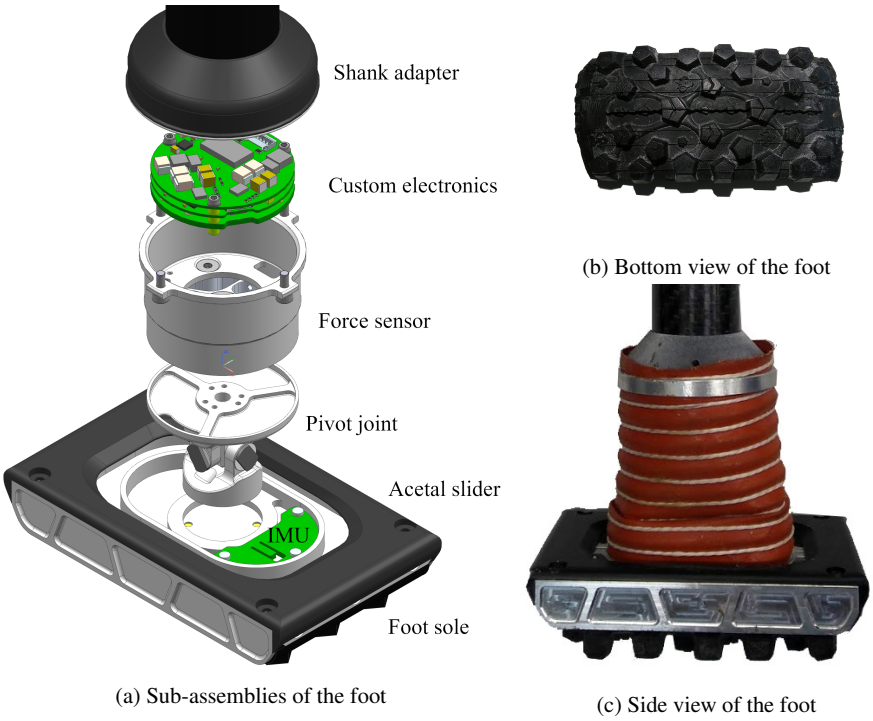

(a) Sub-assemblies of the foot

(b) Bottom view of the foot

(c) Side view of the foot

Fig. 2: Overview of the newly developed foot for sewer inspection.

3) Force sensor: A custom, in-house developed 6-axis force/torque sensor[2] is placed above the pivot joint to measure the forces acting on the foot. It consists of a force sensing element with strain gauges. The sensor is lightweight and robust and allows sensing up to 1000 N along the z-axis and 400 N along the x and y-axis. The maximum torque the sensor can sense is specified as 10 Nm. The accuracy lies within 1.5% of the measured value while the repeatability lies below 0.05%. The sensor is temperature compensated to minimize drift during operation.

4) Custom electronics: The electronics of the foot consists of two IMUs (MPU-9250), a force sensor and a microcontroller board. One of the IMUs is located in the sole, while the other is integrated with the PCB in the shank. Both the IMUs and the force sensor are connected to the microcontroller via the serial peripheral interface bus (SPI). The IMUs are read out with 1 kHz and force measurements are obtained with 400 Hz. The microcontroller board is connected to the robot via EtherCAT and powered through the auxiliary 12 V power line. The custom 6-axis force/torque features a PCB with analog-to-digital converters (ADCs) and a microcontroller that processes the analog signals of the strain gauges. Sensor data is recorded on the high-level side at 400 Hz.

[2] https://www.botasystems.com/

5) Shank: The carbon fiber shank connects the foot to the knee of the robot. The shank is sealed and features a conical slider for protection of the force sensor.

6) Sealing: The joint is protected by thick bellows (visible in Figure 2c), mechanically clamped to the structure and sealed, which improves the ingress protection rating compared to previous work. O-rings and sealants have been used for all the matching surfaces. Water-proof cable glands and connector have been used for the cables.

3 Tactile inspection motion

The scratching motion we use to collect the data needs to be repeatable and reliable across the entire range of possible surface areas. The motion, therefore, needs to be specified in such a way that it can adapt to local terrain geometry and surface roughness. We implemented a Cartesian-space impedance controller [19], which allows a motion design on both force and position level. Specifying and executing these motions was done by extending the free-gait framework [20]. The full sequence of the inspection motion, shown in Figure 3, can be split into several phases.

A predefined position relative to the three stance legs is approached in (a) and contact is established in (b). In (c), a straight line trajectory is followed until a target location (d). In (e) and (f), the foot is re-positioned to return to a nominal stance on four feet. For the part (c) of the inspection motion, where data is collected, the desired end-effector force is computed as seen in the following equation.

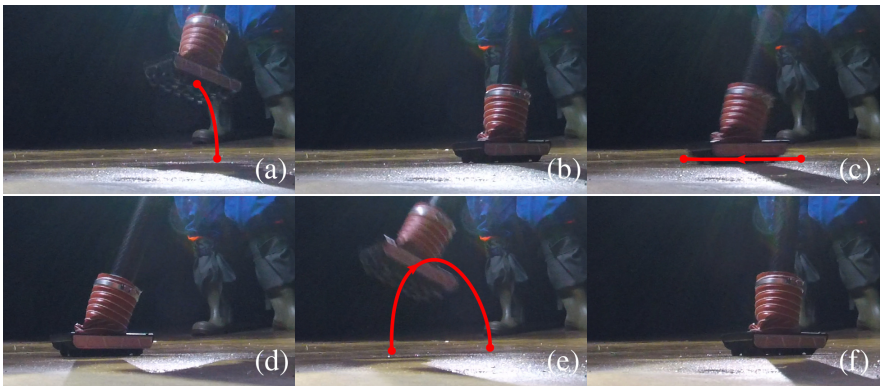

Fig. 3: Picture sequence of the tactile inspection motion with the foot placement phase (a), inspection motion start location (b), main inspection phase (c), motion target (d), re-positioning movement (e), and final position (f).

$$\boldsymbol{f}_{des} = \boldsymbol{f}_{ref} + \boldsymbol{\Lambda}(\boldsymbol{q})\ddot{\boldsymbol{x}}_{ref} + \boldsymbol{K}_p(\boldsymbol{x} - \boldsymbol{x}_{ref}) + \boldsymbol{K}_d(\dot{\boldsymbol{x}} - \dot{\boldsymbol{x}}_{ref}) + c_\mu \frac{\dot{\boldsymbol{x}}_{ref}}{\|\dot{\boldsymbol{x}}_{ref}\|} |\boldsymbol{n}^T \boldsymbol{f}_{ref}|, \quad (1)$$

where $\boldsymbol{f}_{ref}$ is the designed Cartesian end-effector force reference, and $\boldsymbol{x}_{ref}, \dot{\boldsymbol{x}}_{ref}, \ddot{\boldsymbol{x}}_{ref}$ are the designed position, velocity and acceleration references. $\boldsymbol{\Lambda}(\boldsymbol{q})$ is the reflected inertia matrix, which depends on the generalized coordinates $\boldsymbol{q}$. $\boldsymbol{K}_p$ and $\boldsymbol{K}_d$ are the position and velocity gain matrices. Finally, c_μ is a scalar value used to provide a feedforward friction compensation in the direction of the motion, scaled by the reference force along the surface normal, $\boldsymbol{n}$.

For the main part of the inspection motion, we apply a force of 10 N on the surface. The target location is set 100 mm forward and 50 mm sideways from the start location. Together with a total duration of 2 s and an initial and final velocity of zero, a quintic spline interpolation is defined between the start and end location to generate the motion reference. Impedance gains are set with stiffness $\boldsymbol{K}_p = \text{diag}(200, 200, 0)$ in N/m, and damping $\boldsymbol{K}_d = \text{diag}(20, 20, 20)$ in Ns/m.

Friction compensation c_μ was set to 1.0 after experimental tuning in the field. We found the high friction compensation to be important for successful motion execution on the rougher surfaces. The value of 1.0 served as a safe upper bound for the roughest terrain encountered. For more slippery surfaces the compensation is too high, but this does not pose a problem as the damping terms quickly regulate the velocity and stabilize the motion.

4 Sewer inspection with quadruped robots

4.1 Field test campaign

We conducted multiple field test campaigns in the sewage system of Zurich to iterate the hardware, practice operations and collect datasets. Generally, the robot can be easily deployed through a common utility hole (d = 0.8 m). To do so, the robot's legs are tucked up and the system is lowered into the sewer with a tethered rope (Figure 4). During our tests, the robot was operated from a base station which was located outside the sewer, nearby the utility hole.

The base station consists of the operator PC, an additional screen and outlets for electricity and communication links to the robot. Additionally, the base station is easy to transport and quick to set up. A directional Wi-Fi antenna (Ubiquiti airMAX) was deployed into the utility hole via a tripod with reversed column and enabled a reliable communication link to the robot. During the test, an operator stayed in the sewers with a professional inspector and communicated with the robot operator outside via walkie-talkies (Figure 5).

The dataset was collected in two rectangular shaped sewers. Both sewers were accessible through a utility hole and large enough to be traversable by humans. A slight inclination towards the center and towards the direction of flow, resulted in a higher accumulation of water in the center.

Fig. 4: Depiction of the field test setup and the deployment of *ANYmal* into the sewer. The operator base station and warnings signs are visible in the background.

(a) *ANYmal* setup in the sewer

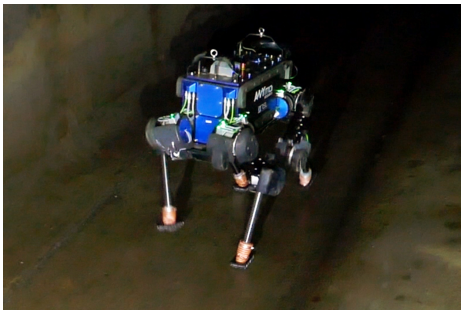

(b) Walking on biofilm

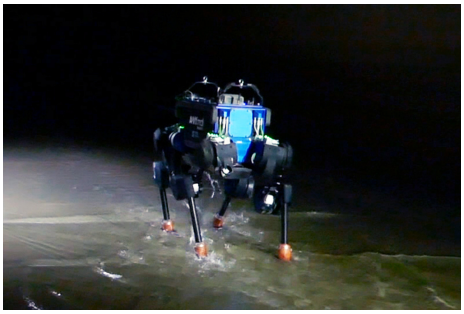

(c) Walking through wastewater

Fig. 5: Depictions of *ANYmal* walking in the sewer. A professional sewer inspector accompanies the testing and assesses the state of the concrete.

Thus, to avoid over-fitting during classification later on, we moved and reoriented the robot frequently to capture different areas and poses of the robot with respect to the sewer floor. In order to construct the dataset, we defined a scale of five condition ratings for the sewers. The scale was developed with professional sewer inspectors who use a similar scheme to assess the state of the sewers.

- **Good:** Smooth concrete, no problems noticeable
- **Satisfactory:** Minor signs of deterioration, increased roughness
- **Fair:** Medium signs of deterioration, increased roughness and scratches/spalling
- **Critical:** Major deterioration noticeable, large cracks, imminent failure
- **Failure:** Loss of structural integrity, leakage

The condition of the concrete we encountered in the sewers ranged from *good* to *fair*, while *critical* or extremely bad structural *failures* were not encountered. In total, we were able to collect 355 samples (*good*: 119 samples, *satisfactory*: 79 samples, *fair*: 157 samples) in different parts of the sewers, which were classified together with a professional sewer inspector who provided the ground truth. The dataset named *STINK* (Sewer Terrain Inspection Knowledge) is openly available[3].

4.2 Classifying concrete deterioration

We chose a machine learning approach to capture and classify the diverse appearance of concrete deterioration together with the varying environmental conditions. As mentioned, the surface condition is not only expressed by the roughness of the concrete, but also by macroscopic features such as holes, scratches or cracks. At the same time, the surface can be dry, wet, submerged and/or covered by a biofilm (Figure 6).

(a) good state, water (b) satisfactory state, biofilm (c) fair state, wet

Fig. 6: An exemplary set of pictures illustrating the various surface conditions encountered in the sewers.

[3] DOI: 10.3929/ethz-b-000336822

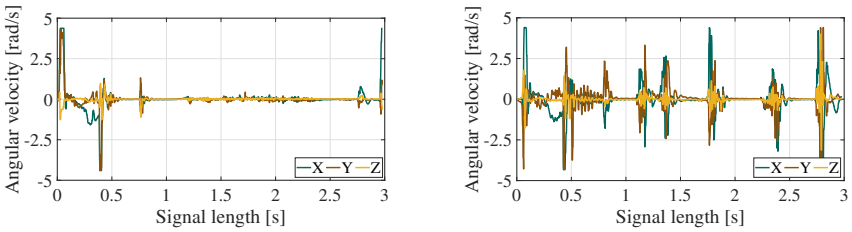

(a) Concrete in good condition (b) Concrete in fair condition

Fig. 7: Comparing the angular velocities of two samples recorded by the foot sole IMU show a correlation between signal magnitudes and concrete deterioration.

We extracted the raw sensor data acquired while performing the inspection motion in the sewers without further cleanup or filtering. The acquired data consists of 18 signals (Force/Torque, IMU shank (linear acceleration/angular velocity), IMU sole (linear acceleration/angular velocity).

The data is cropped to three seconds, starting at the point of first lift-off (Figure 3a). The raw sensor signals showed a correlation between signal magnitudes and concrete deterioration level (Figure 7). Thus, each sensor signal was decomposed using a fast Fourier transform (FFT) to express the vibrations in the frequency domain. Next, we took the magnitude of the frequency components and standardized the data to have zero mean and unit standard deviation. Last, the dimensionality of the feature vector was reduced with a principal component analysis (PCA) with 30 principal components.

We trained a support vector machine (SVM) with linear Kernel (LIBSVM for Matlab [21]) on randomly chosen 70% of the dataset (248 Samples). The linear Kernel was chosen since it resulted in high overall accuracy. More complex, non-linear or radial basis Kernels were omitted since they increase the chance of overfitting while only supplying a marginal increase in performance. We trained on the data using five-fold cross-validation combined with a grid search to find an optimal C-setting. We trained three binary one-vs-all classifiers to solve the multi-class problem. The accuracy was determined by predicting the degradation level of the remaining 30% of the dataset (107 Samples), which was left out during training.

4.3 Classification results

We classified the deterioration levels with good accuracy and achieved an overall classification accuracy of more than 92% on the three assigned classes. Comparing the individual sensor contributions to the classification performance shows, that the IMU's, and especially the IMU in the sole provide a high accuracy (Table 1). The IMU in the shank achieves a slightly lower accuracy compared to the IMU in the sole, which experiences higher excitations when slipping over rough surfaces.

Table 1: Classification accuracy related to selected sensor signals (average performance over 25 evaluations).

Sensor signal	Classification accuracy			
	Poor	Fair	Good	Overall
Force	92.9%	68.8%	87.0%	**82.9%**
Torque	92.9%	65.1%	88.0%	**82.0%**
Force & Torque	88.5%	72.8%	81.5%	**80.9%**
IMU Sole (lin acc)	93.2%	83.8%	93.1%	**90.0%**
IMU Sole (ang vel)	93.0%	88.0%	95.3%	**92.1%**
IMU Sole	93.7%	84.3%	92.3%	**90.1%**
IMU Shank (lin acc)	91.8%	84.9%	92.1%	**89.6%**
IMU Shank (ang vel)	90.0%	65.1%	91.2%	**82.1%**
IMU Shank	89.8%	84.6%	92.2%	**88.9%**
IMU Sole & Shank	95.1%	88.2%	95.2%	**92.8%**
F/T + IMU Sole & Shank	94.4%	87.7%	93.9%	**92.0%**

The contribution of the Force/Torque sensor to the classification accuracy is lower compared to the IMU's. Nevertheless, high accuracy was achieved when using all available sensors, but also a minimal setup consisting of only the IMU in the sole achieves a good performance. This matches previous findings on planetary soil classification [15].

Performing the classification with the two IMU's resulted in the highest accuracy and further investigations were performed with this setup. Investigating the misclassified samples showed no specific preference to location or surface condition. Fewer samples were available for the *satisfactory* class compared to the *good* and *fair* class, which might explain the general lower classification performance on the validation set. An exemplary confusion matrix for evaluating the validation set can be seen in Figure 8. Investigating the sampling time shows that the signals should be captured for at least one second after the motion is initiated to achieve a high classification accuracy. Longer sampling times increase the performance only marginally. In practice, human inspectors are scratching the sewer frequently with their feet during a walk through to get a better understanding of the damages.

The same approach can be followed by the robot to increase the accuracy and confidence in the classification. While a critical or fatal concrete condition was not encountered during the acquisition of the dataset, we are confident that these could also be detected with this approach.

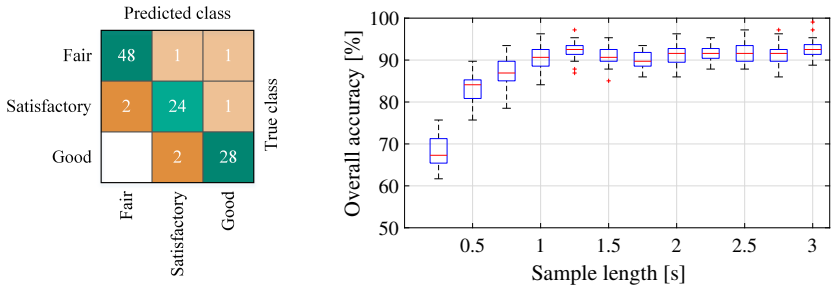

(a) Exemplary confusion matrix (b) Accuracy increase over signal duration

Fig. 8: Few misclassification events occur between classes. Correlation between classification accuracy and signal length indicates that samples should be collected for at least one second after initializing the inspection motion.

5 Conclusion

We show how a legged robot inspects concrete deterioration in medium to large sewers. Through multiple consecutive field test campaigns, we developed a method which allows the quadruped robot *ANYmal* to walk in the sewage system of Zurich, perform a tactile inspection of the concrete, and classify the deterioration level. To cope with the wet and slippery environment in the sewer environment, we have developed adaptive planar feet. Through an impedance controlled scratching motion, the robot is able to probe the terrain with one of its limbs, while maintaining balance with the other. We acquired and open sourced a dataset with 355 samples during two consecutive days in the sewers. Training a support vector machine on the dataset allowed us to predict the current state of the concrete deterioration within three classes with over 92% accuracy. Analysis of the data shows that also a minimal set of sensors is sufficient for classification.

While the inspection approach worked well, further improvements are required to increase robustness and reliability. First, the system needs to be able to traverse several hundred meters autonomously through inclined and partially flooded sewers to demonstrate a similar capability to a human inspector. Secondly, more data needs to be collected to confirm robustness on a diversified set of sewers, improve accuracy, and eventually precision of the prediction. Overall, we believe that these shortcomings will be overcome and that legged robots will become a valuable partner in the inspection of sewers.

Acknowledgements The authors want to thank Roman Weiss and his colleagues from *ERZ - Entsorgung + Recycling Zurich* for their support during this study. This work has been supported by the European Unions Horizon 2020 research and innovation programme under grant agreement No 780883 and by the European Space Agency (ESA) and Airbus DS in the framework of the Network Partnering Initiative 481-2016. This work has been conducted as part of ANYmal Research, a community to advance legged robotics.

References

1. Christian Berger and Christian Falk. *Zustand der Kanalisation in Deutschland - Ergebnisse der DWA-Umfrage 2009*. Deutsche Vereinigung für Wasserwirtschaft, Abwasser und Abfall e. V. (DWA), Hennef, 2009.
2. Cornelia Dyk and Johannes Lohaus. *Der Zustand der Kanalisation in Deutschland - Ergebnisse der ATV-Umfrage 1997*. ATV (Abwassertechnische Vereinigung e.V.), Hennef, 1997.
3. Christian Berger, Christian Falk, Friedrich Hetzel, Johannes Pinnekamp, Silke Roder, and Jan Philip Ruppelt. *Zustand der Kanalisation in Deutschland - Ergebnisse der DWA-Umfrage 2015*. Deutsche Vereinigung für Wasserwirtschaft, Abwasser und Abfall e. V. (DWA), Hennef, 2016.
4. A. K. Parande, P. L. Ramsamy, S. Ethirajan, C. R. K. Rao, and N. Palanisamy. Deterioration of reinforced concrete in sewer environments. *Proceedings of the Institution of Civil Engineers - Municipal Engineer*, 159(1):11–20, 2006.
5. Emilie Hudon, Saeed Mirza, and Dominic Frigon. Biodeterioration of concrete sewer pipes: State of the art and research needs. *Journal of Pipeline Systems Engineering and Practice*, 2(2):42–52, 2011.
6. T. Wells and R.E. Melchers. Modelling concrete deterioration in sewers using theory and field observations. *Cement and Concrete Research*, 77:82 – 96, 2015.
7. Josep M. Mirats Tur and William Garthwaite. Robotic devices for water main in-pipe inspection: A survey. *Journal of Field Robotics*, 27(4):491–508, 2010.
8. Christoph Walter, Jos Saenz, Norbert Elkmann, Heiko Althoff, Sven Kutzner, and Thomas Stuerze. Design considerations of robotic system for cleaning and inspection of large-diameter sewers. *Journal of Field Robotics*, 29(1):186–214, 2012.
9. Redzone robotics responder description. https://www.redzone.com/technology/responder. Accessed: 2019-04-07.
10. G. Seet, S.H. Yeo, W.C. Law, Burhan, C.Y. Wong, S. Sapari, and K.K. Liau. Design of tunnel inspection robot for large diameter sewers. *Procedia Computer Science*, 133:984 – 990, 2018. International Conference on Robotics and Smart Manufacturing (RoSMa2018).
11. Pure technologies smartball description. https://puretechltd.com/technology/smartball-leak-detection/. Accessed: 2019-04-07.
12. M. Hutter, R. Diethelm, S. Bachmann, P. Fankhauser, C. Gehring, V. Tsounis, A. Lauber, F. Guenther, M. Bjelonic, L. Isler, H. Kolvenbach, K. Meyer, and M. Hoepflinger. Towards a Generic Solution for Inspection of Industrial Sites. In *Field and Service Robots (FSR)*, 2017.
13. C. Dario Bellicoso, Marko Bjelonic, Lorenz Wellhausen, Kai Holtmann, Fabian Günther, Marco Tranzatto, Peter Fankhauser, and Marco Hutter. Advances in real-world applications for legged robots. *Journal of Field Robotics*, 35(8):1311–1326, 2018.
14. M. A. Hoepflinger, C. D. Remy, M. Hutter, L. Spinello, and R. Siegwart. Haptic terrain classification for legged robots. In *2010 IEEE International Conference on Robotics and Automation*, pages 2828–2833, May 2010.
15. H. Kolvenbach, C. Bärtschi, L. Wellhausen, R. Grandia, and M. Hutter. Haptic inspection of planetary soils with legged robots. *IEEE Robotics and Automation Letters*, 4(2):1626–1632, April 2019.
16. M. Hutter, C. Gehring, A. Lauber, F. Gunther, C. D. Bellicoso, V. Tsounis, P. Fankhauser, R. Diethelm, S. Bachmann, M. Bloesch, H. Kolvenbach, M. Bjelonic, L. Isler, and K. Meyer. Anymal - toward legged robots for harsh environments. *Advanced Robotics*, 31(17):918–931, 2017.
17. Hendrik Kolvenbach and Marco Hutter. Life extension: An autonomous docking station for recharging quadrupedal robots. In *Field and Service Robotics*, pages 545–557, Cham, 2018. Springer International Publishing.
18. Roman Käslin, Hendrik Kolvenbach, Laura Paez, Klajd Lika, and Marco Hutter. Towards a passive adaptive planar foot with ground orientation and contact force sensing for legged robots. *IEEE/RSJ International Conference on Intelligent Robots and Systems (IROS 2018)*, October 2018.

19. Oussama Khatib. A unified approach for motion and force control of robot manipulators: The operational space formulation. *IEEE Journal on Robotics and Automation*, 3(1):43–53, 1987.
20. P. Fankhauser, C. Dario Bellicoso, C. Gehring, R. Dub, A. Gawel, and M. Hutter. Free gait: An architecture for the versatile control of legged robots. In *2016 IEEE-RAS 16th International Conference on Humanoid Robots (Humanoids)*, pages 1052–1058, Nov 2016.
21. Chih-Chung Chang and Chih-Jen Lin. LIBSVM: A library for support vector machines. *ACM Transactions on Intelligent Systems and Technology*, 2:27:1–27:27, 2011. Software available at http://www.csie.ntu.edu.tw/ cjlin/libsvm.